Protein Science (1994), *3*:1098–1107. Cambridge University Press. Printed in the USA.

Crystal structure of inorganic pyrophosphatase from *Thermus thermophilus*

ALEXEI TEPLYAKOV,[1] GALYA OBMOLOVA,[1] KEITH S. WILSON,[1] KEISUKE ISHII,[2] HIROYUKI KAJI,[2] TATSUYA SAMEJIMA,[2] AND INNA KURANOVA[3]

[1] European Molecular Biology Laboratory, % DESY, Notkestr. 85, 22603 Hamburg, Germany
[2] Department of Chemistry, College of Science and Engineering, Aoyama Gakuin University, Tokyo 157, Japan
[3] Institute of Crystallography, Leninsky pr. 59, Moscow 117333, Russia

(RECEIVED February 2, 1994; ACCEPTED April 19, 1994)

Abstract

The 3-dimensional structure of inorganic pyrophosphatase from *Thermus thermophilus* (T-PPase) has been determined by X-ray diffraction at 2.0 Å resolution and refined to $R = 15.3\%$. The structure consists of an antiparallel closed β-sheet and 2 α-helices and resembles that of the yeast enzyme in spite of the large difference in size (174 and 286 residues, respectively), little sequence similarity beyond the active center (about 20%), and different oligomeric organization (hexameric and dimeric, respectively). The similarity of the polypeptide folding in the 2 PPases provides a very strong argument in favor of an evolutionary relationship between the yeast and bacterial enzymes. The same Greek-key topology of the 5-stranded β-barrel was found in the OB-fold proteins, the bacteriophage gene-5 DNA-binding protein, toxic-shock syndrome toxin-1, and the major cold-shock protein of *Bacillus subtilis*. Moreover, all known nucleotide-binding sites in these proteins are located on the same side of the β-barrel as the active center in T-PPase. Analysis of the active center of T-PPase revealed 17 residues of potential functional importance, 16 of which are strictly conserved in all sequences of soluble PPases. Their possible role in the catalytic mechanism is discussed on the basis of the present crystal structure and with respect to site-directed mutagenesis studies on the *Escherichia coli* enzyme. The observed oligomeric organization of T-PPase allows us to suggest a possible mechanism for the allosteric regulation of hexameric PPases.

Keywords: active center; allosteric regulation; crystal structure; divergent evolution; inorganic pyrophosphatase; *Thermus thermophilus*

Inorganic pyrophosphatase (pyrophosphate phosphohydrolase, EC 3.6.1.1) catalyzes hydrolysis of inorganic pyrophosphate as well as oxygen exchange between water and inorganic phosphate and PP_i:P_i equilibration (Butler, 1971; Josse & Wong, 1971; Lahti, 1983). PP_i is a by-product of numerous important reactions including nucleic acid polymerization, coenzyme synthesis, and amino acid and fatty acid activation. By cleaving PP_i, the enzyme shifts the overall equilibrium in favor of synthesis and thus plays a vital role in the cell. PPase might also play a role in evolutionary events by affecting the accuracy of DNA copying during chromosome duplication (Herbomel & Ninio, 1980). On the other hand, PPase provides the simplest model reaction for studies on energy transduction at the level of phosphoanhydride bond formation and breakdown, and the data derived might be useful for understanding the mechanism of both PP_i and ATP synthesis.

PPase is present in virtually any cell—animal, vegetable, or microbial—and is mainly localized in the cytosol. All cytosolic PPases isolated so far require divalent cations (preferably Mg^{2+}) for activity and have similar catalytic properties but different quaternary structures. Most prokaryotic PPases form hexamers of molecular weight of 120 kDa, whereas eukaryotic enzymes are homodimers of 30–35-kDa subunits. PPases from *Escherichia coli* and from baker's yeast are the best studied members of the 2 groups (Cooperman et al., 1992). The amino acid sequence identity between them is only about 25%. Extensive chemical modification studies indicated residues that might be essential for catalytic activity and substrate binding (Cooperman, 1982). The genes encoding these PPases have been cloned (Kolakowski et al., 1988; Lahti et al., 1988) and site-directed mutagenesis studies of the catalytic mechanism are now under way (Lahti et al., 1990b, 1991). Thus, detailed 3-dimensional information on PPases is urgently required. The only crystal struc-

Reprint requests to: A. Teplyakov, European Molecular Biology Laboratory, % DESY, Notkestr. 85, 22603 Hamburg, Germany; e-mail: alex@embl-hamburg.de.

Abbreviations: PP_i, inorganic pyrophosphate; P_i, inorganic phosphate; PPase, inorganic pyrophosphatase. B-PPase, E-PPase, P-PPase, T-PPase, and Y-PPase are the enzymes from *Bacillus stearothermophilus*, *Escherichia coli*, PS-3, *Thermus thermophilus*, and yeast, respectively.

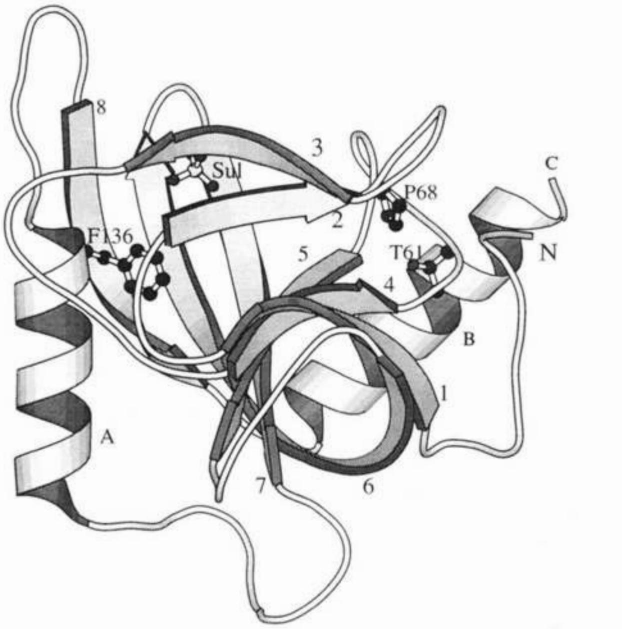

Fig. 1. Ribbon representation of the T-PPase subunit produced with MOLSCRIPT (Kraulis, 1991). The N- and C-termini and the secondary-structure elements are labeled: β-strands with numbers from 1 to 8, α-helices with letters A and B. The location of the active center is indicated by a sulfate. Conservative residues outside the active center are shown (see "Structural role of conserved amino acids").

ture determined to date is that of Y-PPase. It has been solved by multiple isomorphous replacement at 3.0 Å resolution (Kuranova et al., 1983; Terzyan et al., 1984), and a preliminary report on the refinement at 2.35 Å resolution has been published (Chirgadze et al., 1991).

As a step toward understanding the general principles of catalysis by PPases and evolutionary relationships between the members of this family of enzymes, we have determined the 3-dimensional structure of PPase from *Thermus thermophilus*. The 2.0-Å crystal structure of T-PPase described in this paper can serve as a template model for studies of other prokaryotic PPases because they are highly homologous in terms of amino acid sequence.

Results and discussion

Structure of T-PPase subunit and comparison to Y-PPase

The polypeptide chain of T-PPase is folded into a globular subunit of size of $28 \times 40 \times 42$ Å^3. The core of the subunit is composed of a highly twisted 6-stranded antiparallel β-sheet, which forms a 5-stranded β-barrel (strands 1, 4, 5, 6, and 7; see Fig. 1 and Kinemage 1). Two α-helices (A and B) and a long β-hairpin (strands 2 and 3) surround the sheet. Residues preceding and following helix A form consecutive β-turns and can be described as distorted 3_{10}-helices. In total there are 4 short helices 3_{10}, 6 β-turns of type I, and 2 of type II in the T-PPase structure. Both β-turns of type II (residues 23–26 and 80–83) contain glycines in the $(i+2)$ position. The secondary-structure elements (Fig. 2) have been determined on the basis of main-chain hydrogen bonds and conformational angles ϕ and ψ, with the help of the program DSSP (Kabsch & Sander, 1983). Classification of β-turns follows Richardson (1981). The secondary structure revealed by X-ray analysis is in agreement with the optical rotatory dispersion data measured on E-PPase (Burton et al., 1970), which suggested little α-helical content.

A closed β-sheet structure can be described by 2 integral parameters: the number of strands, n, and the shear number, S (McLachlan, 1979). The β-barrel in T-PPase has $n = 5$ and $S = 8$ (Fig. 3). The mean radius of the barrel (5.8 Å) and the average inclination of the strands to the barrel axis (50°) calculated from these parameters agree well with the observed values of 6 Å and 50°, respectively. The small radius of the barrel requires a strong coiling of the β-strands, which is promoted by β-bulges in strands 1 and 7 at positions 21 and 90. The glycine residue in

```
                β1    10     β2  20        30         40   β3    50       β4 60
Y-PPase   TYTTRQIGAKNTLEYKVYIEKDGKPVSAFHDIPLYADKENNIFNMVVEIP-RWTNAKLEITKE
E-PPase                             SLLNVPAG-KDLPEDIYVVIEIPANADPIKYEIDKE
T-PPase                            ANLKSLPVG-DKAPEVVHMVIEVP-RGSGNKYEYDPD
                                     §       10     β1 20          β2

             β5         80         90 β6      100        110       β7
Y-PPase   ETLNPIIQDTKKGKLRFVRNCFPHHGYIHNYGAFPQTWEDPNVSHPETKAVGDNDPIDVLEIG
E-PPase   S--GALFVD------RFMSTA---MFYPCNYGYINHTLSL------------DGDPVDVLVPT
T-PPase   L--GAIKLD------RVLPGA---QFYPGDYGFIPSTLAE------------DGDPLDGLVLS
             40   β3              50   β4   60                      70 β5

              130    β8 140         150  β9     160     §      §  α     180 αA
Y-PPase   ETIAYTGQVKQVKALGIMALLDEGETDWKVIAIDIND--PLAPKLNDIEDVEKYFPGLLRATN
E-PPase   PYPLQPGSVIRCRPVGVLKMTDEAGEDAKLVAVPHSKLSKEYDHIKDVNDLP---ELLKAQIA
T-PPase   TYPLLPGVVVEVRVVGLLLMEDEKGGDAKVIGVVAED--QRLDHIQDIGDVP---EGVKQEIQ
             80     β6 90          100  β7    110    §      120§      αA 130

          αA 190  §          β10  §   210         220 αB         230       240
Y-PPase   EWFRIYKIPD---GKPENQFAFSGEAKNKKYALDIIKETHDSWKQLIAGKSSDSKGIDLTNVT
E-PPase   HFFEHYKDLE--KGKWVKV----EGWENAEAAKAEIVASFERAKNK
T-PPase   HFFETYKALEAKKGKWVKV----TGWRDRKAALEEVRACIARYKG
           αA    140 §    150   β8           160   αB   170

             250      §260   β11   270   §     280
Y-PPase   LPDTPTYSKAASDAIPPASPKADAPIDKSIDKWFFISGSV
```

Fig. 2. Amino acid sequence alignment of PPases from *S. cerevisiae* (Y-PPase), *E. coli* (E-PPase), and *T. thermophilus* (T-PPase) based on the 3-dimensional superposition of T-PPase and Y-PPase structures. Amino acids conserved in all soluble PPases are written in boldface. Secondary-structure elements and residue numbers are indicated for T-PPase (below sequences) and Y-PPase (above sequences). α, α-helix; §, helix 3_{10}; β, β-strand.

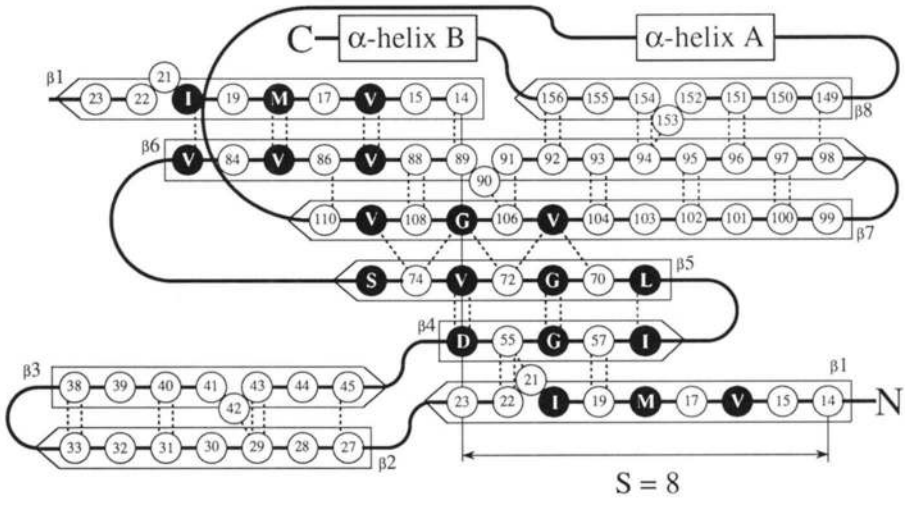

Fig. 3. Topology of β-structure in the T-PPase subunit. The β-barrel is unrolled with the first strand repeated twice on both sides to show its shear number $S = 8$. Hydrogen bonds are shown by dotted lines. Residues forming the interior of the barrel are shown as black circles with 1-letter amino acid symbols.

position 56 provides conformational flexibility for bending of strands 4 and 5. The interior of the β-barrel is tightly packed with hydrophobic side chains. The only exception is the pair Asp 54–Ser 75, with a hydrogen bond between their side chains. The β-barrel is closed at the bottom by the amphipathic helix B, which donates residues Ala 161 and Val 165 to the interior of the barrel. A short loop connecting strands 5 and 6 closes the top side of the barrel and contributes Leu 79 to the hydrophobic core. Structural determinants of the β-barrel discussed here support recent findings of Murzin (1993) based on a comparison of 4 nonhomologous proteins containing 5-stranded closed β-sheets.

The structure of the T-PPase subunit is similar to that of Y-PPase (Fig. 4; Kinemage 1). Their superposition based on all 174 common C_α atoms (Fig. 2) gave an average deviation of 1.98 Å. When atoms deviating by more than 2 Å were excluded from the comparison, the structures could be superimposed with an average deviation of 0.94 Å for the remaining 126 C_α atoms. The Y-PPase subunit consists of 2 β-sheets (β-strands 1, 2, 4, 5, and 11, and β-strands 3, 6, 7, 8, 9, and 10) and 2 long α-helices (A and B). The most conserved regions of the structure in terms of the spatial superposition of the 2 PPases are the β-barrel and α-helix A, whereas helix B is tilted by 10°. Parts of the sequence corresponding to the β-strands 1, 2, and 11 are missing in T-PPase, so that it contains only the β-hairpin equivalent to the strands 4 and 5 of Y-PPase. Irregular fragments of the chain show significant conformational freedom deviating by up to 4 Å between the 2 structures.

If one describes the shape of the Y-PPase subunit as a hat, then the T-PPase subunit can be obtained by removing the brim of this hat (Fig. 4; Kinemage 1). The active site in both PPases is located inside the crown. The brim in the Y-PPase hat is formed by the N- and C-terminal fragments of the chain and insertions in the loop regions and can be removed without disturbing the rest of the structure. The similarity of the polypeptide folding in T-PPase and Y-PPase provides a very strong argument in favor of an evolutionary relationship between the yeast and bacterial enzymes. Taking into account the much higher degree of sequence homology between prokaryotic PPases (43–48% identity) as well as similar molecular weights and oligomeric organization, one can expect significant similarity of their tertiary and quaternary structures. The 3-dimensional similarity of T-PPase and E-PPase is also supported by the fact that their crystals are isomorphous (Moroz et al., 1991).

Fig. 4. Superposition of T-PPase (dark coil) and Y-PPase (light coil). Residue numbers are shown for Y-PPase at the insertion sites. The location of the active center is indicated by a sulfate.

Comparison with topologically similar proteins

The 5-stranded β-barrel structure has been found in the major cold-shock protein from *Bacillus subtilis* (Schindelin et al., 1993; Schnuchel et al., 1993), the gene-5 DNA-binding protein from bacteriophage fd (Brayer & McPherson, 1983), toxic-shock syndrome toxin-1 (Prasad et al., 1993; Acharya et al., 1994), and the OB-fold proteins (Murzin, 1993), which include staphylococcal nuclease, the anticodon-binding domain of yeast asp-tRNA synthetase, B-subunits of heat-labile enterotoxin and verotoxin from *E. coli*, and the N-terminal domain of staphylococcal enterotoxin B. Superposition of T-PPase and staphylococcal nuclease, a representative of the OB-fold proteins, yields an average deviation of 1.5 Å for the 33 C_α atoms of their barrels used for comparison. All proteins reveal the same Greek-key topology of the barrel. The rest of the structure is very different in these proteins. In spite of the lack of sequence homology, the oligonucleotide-binding site in the OB-fold proteins and proposed binding sites in the gene-5 and cold-shock proteins are located on the same side of the β-barrel as the active centers in T-PPase and Y-PPase, i.e., on the face formed by strands 5 and 7 (Fig. 1; Kinemage 1). Two explanations of the phenomenon are possible. One is the existence of a common ancestor of soluble PPases and some of the nucleotide-binding proteins. This is, however, unlikely because the OB-fold proteins have a different shear number of the β-barrel ($S = 10$) that implies different packing inside the barrel as compared to the PPases. Another explanation assumes that they evolved independently to the β-barrel as one of the stable types of the structure. The shallow groove on the barrel surface surrounded by loops forms a potential binding site, which was edited by evolution for different ligands.

In the recent classification of α+β folds (Orengo & Thornton, 1993) Y-PPase was placed in a group of large complex molecules. Taking into account the structural and functional similarities between soluble PPases, it seems reasonable to consider them as members of 1 group in spite of the different size of the molecules. The principal element of their structure is the 5-stranded β-barrel. Therefore they can form a subgroup of α-β-roll proteins.

Active center and catalytic mechanism

The active-site pocket is located between the β-barrel and helix A (on the top of Fig. 1; Kinemage 1). It is a hemispherical concave with a diameter of 10 Å as measured between side chains of residues aligning the pocket. The large active center of PPase is supposed to accommodate at least 3 Mg^{2+} ions and PP_i or 2 P_i (Bond et al., 1980; Knight et al., 1984; Baykov et al., 1989, 1990).

X-ray analysis of Y-PPase (Kuranova et al., 1983; Terzyan et al., 1984) revealed 17 residues that might be involved in Mg^{2+} and PP_i binding. Fifteen of them appeared to be conserved in all sequences of soluble PPases known to date (Fig. 2). All 15 (Glu 21, Lys 29, Glu 31, Arg 3, Tyr 51, Tyr 55, Asp 65, Asp 67, Asp 70, Asp 97, Asp 102, Lys 104, Tyr 139, Lys 140, and Lys 148) reside in the active-site cavity of T-PPase (Fig. 5; Kinemage 2). The other 2 putative functional residues, Glu 148 and Glu 150 of Y-PPase, belong to the "acidic hexapeptide" 147–152 (residues 97–102 in T-PPase), which could be locally aligned to match glutamate residues in different PPases (Lahti et al., 1990a). The common feature of this fragment is that all PPases contain Glu and Gly amino acids although the sequences are not strictly conserved. The "acidic hexapeptide" forms a short loop between β-strands 6 and 7. We suppose that glutamic acid in either of the positions from 98 to 100 can take part in the active-center interactions due to the flexibility of the loop provided by glycine residues. In T-PPase the electron density for this region is weak and discontinuous and the atomic *B*-factors are the highest for the molecule (Fig. 10). Gly 100 has a conformation forbidden for non-glycine residues, with $\phi = 168°$ and $\psi = -150°$ (Fig. 9). T-PPase contains Glu in position 98, which is located at the active center. The fact that some PPases contain, like T-PPase, only 1 Glu in the "acidic hexapeptide" implies that the second Glu is not essential for activity.

Crystal structure of T-PPase reveals 1 more residue, Asp 42, which may play a role in enzyme–substrate interactions due to its location in the active center. It is strictly conserved in sequences of all PPases. As discussed below, Asp 42 might support the correct orientation of the essential arginine upon substrate binding. Thus, there are 17 residues of potential functional importance selected on the basis of the T-PPase atomic model. In terms of the secondary structure, they are distributed over all 8 β-strands of 1 subunit. Neither helices nor other subunits donate residues to the active center. The functional residues are grouped into short pieces of the polypeptide chain that correspond to the extended regions of similarity found by Lahti et al. (1990a) for Y-PPase and E-PPase.

The bottom of the active-site cavity is formed by a cluster of aromatic amino acids Tyr 51, Pro 52, Tyr 55, Phe 135, Phe 136, and Tyr 139. The tyrosines and Phe 136 are strictly conserved

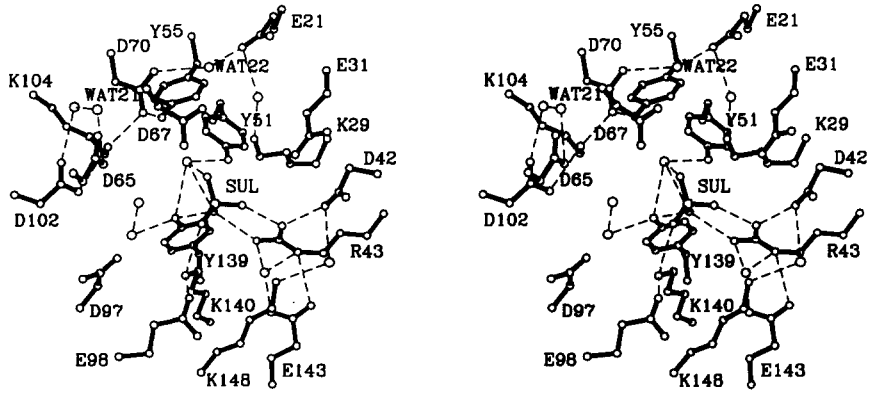

Fig. 5. Active center of T-PPase. Only side chains of amino acid residues are shown. Water molecules are shown as circles. Hydrogen bonds are indicated by dashed lines.

Table 1. *Hydrogen bonds formed by sulfate the active site of T-PPase*

Sulfate atom	Ligand	Distance (Å)
O1	NH1 Arg 43	2.88
O2	NH2 Arg 43	3.12
O2	OH Tyr 139	2.54
O2	O Wat 16	3.13
O3	O Wat 16	2.78
O3	NZ Lys 29	3.22
O4	NZ Lys 140	2.99

in PPases; Pro 52 and Phe 135 are conserved in prokaryotic PPases and replaced, respectively, by Ile and Trp in eukaryotic enzymes. The 3 tyrosines point their hydroxyl groups toward the active center. Adjacent to this cluster is a group of hydrophobic residues Leu 93, Met 95, and Val 152. The sulfhydryl group of Met 95 reaches the solvent-accessible surface of the cavity. However, because this methionine is not conserved in all PPases, its role in the active center might be restricted to maintaining a hydrophobic environment of essential tyrosines rather than a direct interaction with a substrate.

The other 14 residues in the active site are all charged under physiological conditions. The basic amino acids Lys 29, Arg 43, Lys 140, and Lys 148 are clustered at 1 side of the cavity. Other walls are lined with acidic amino acids in the shape of a horseshoe. There is only 1 positive charge between them, which belongs to Lys 104. A possible role of Lys 104, as can be judged from its location, is to stabilize the structure by bridging to the acidic residues (Asp 70 and Asp 102) in the apo-enzyme (Fig. 5; Kinemage 2). Similarly, a hydrogen bond between Glu 98 and Lys 140 might stabilize the structure in the absence of a substrate. Glu 98 and Lys 104 were shown by site-directed mutagenesis to be important for the structural integrity of E-PPase (Lahti et al., 1990b). The distribution of charged residues suggests that the Mg^{2+}-binding sites are most likely located at the acidic cluster, whereas the binding site of PP_i is related to the basic cluster. Cations would support the formation of the PP_i binding site by shielding the negative charge of dicarbonic acids.

In the absence of a substrate, a sulfate ion occupies the active site due to excess of sulfate in the crystallization solution. It was refined with unit occupancy and has an average *B*-factor of 27.4 Å. Sulfate oxygens form hydrogen bonds to the side chains of Lys 29, Arg 43, Tyr 139, and Lys 140 (Fig. 5; Kinemage 2; Table 1). In spite of differences in the electronic structure of sulfate and phosphate, the position of the sulfate apparently shows the electrostatically favorable binding site for an anion. Moreover, the location of the sulfate corresponds to the higher affinity phosphate bound in the Y-PPase crystal complexes with $CaPP_i$ (Kuranova et al., 1983) and MnP_i (Chirgadze et al., 1991). It is also consistent with the proposed role of Arg 43 (Arg 77 in Y-PPase) in substrate binding, which is thought to interact with the leaving phosphoryl group (Cooperman et al., 1981). Finally, the true PP_i substrate might be completely or partially deprotonated (Cooperman, 1982). These considerations lead to the conclusion that in spite of differences in the electronic structure, the observed binding mode of the sulfate can mimic that of a phosphate.

There are several peaks of electron density in the active center that could be treated as water molecules or cations. The crystallization solution contained Mg^{2+} at a concentration of 2 mM. Because Mg^{2+} has almost the same diffraction power as oxygen, the discrimination between them can only be based on the distances to and the character of the ligands. Among all peaks, 2 could be thought of as possible cation-binding sites due to their location within the acidic cluster. Water molecules placed in these peaks have *B*-factors of 22.0 (Wat 21) and 27.0 $Å^2$ (Wat 22). Wat 21 is coordinated to the carboxyl oxygens of Asp 65, carbonyl oxygen of Pro 68, and a water molecule (Fig. 5; Kinemage 2). Wat 22 bridges the carboxyl groups of Glu 21 and Asp 70. Distances to the ligands (2.7–3.1 Å) indicate hydrogen-bonded water molecules rather than magnesium ions, for which the distances should be considerably shorter. This result is somewhat unexpected because the enzyme preparation from *T. thermophilus* contains divalent ions that could be removed only by EDTA (Höhne et al., 1988). Without cations, the aspartate and glutamate residues in the active site show significant mobility as indicated by weak electron density for their side chains (Fig. 6) and reflected by the relatively high *B*-factors. In contrast, lysine and arginine residues have well-defined conformations.

Shestakov et al. (1990) reported the presence of tightly bound ("structural") PP_i in E-PPase and T-PPase, which could not be

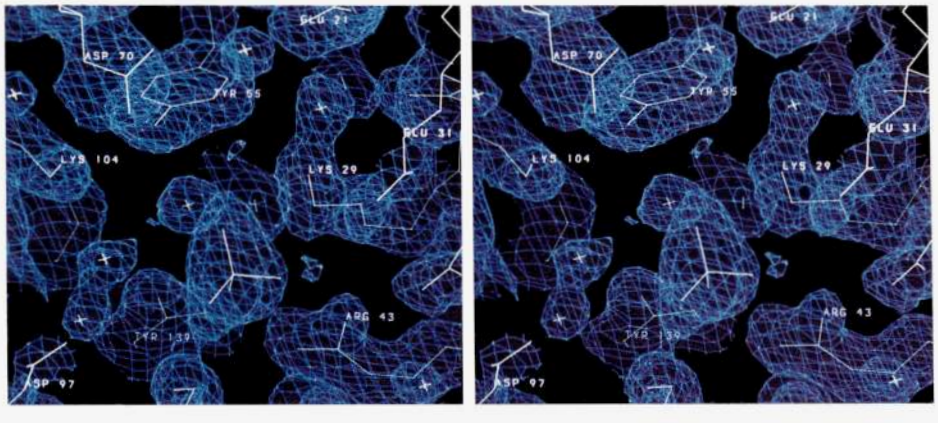

Fig. 6. Electron density in the active center of T-PPase. The map is calculated with coefficients $(3F_o - 2F_c)$ and contoured at the 1.5σ level ($0.6e/Å^3$).

removed without denaturation of the enzyme and which was thought of as a common feature of prokaryotic PPases. The lack of exchange between endogenous PP_i and medium P_i led to the proposal of a "regulatory" binding site of PP_i different from the active site. We were not able to detect any traces of "structural" PP_i either in the active center or elsewhere in the crystal structure of T-PPase.

Four residues, Lys 56 (Komissarov et al., 1985), Arg 78 (Bond et al., 1980), Tyr 89 (Raznikov et al., 1992b), and Glu 150 (Gonzalez & Cooperman, 1986) in Y-PPase, and Lys 29 (Komissarov et al., 1987) and Glu 98 (Raznikov et al., 1992a) in E-PPase have been implicated by chemical modification as being essential for enzymatic activity. Tyr 89 (Tyr 51 in T-PPase numbering) was proposed to serve as a proton donor for P_i releasing during PP_i hydrolysis (Raznikov et al., 1992b). However, E-PPase variant Y51F has a residual activity of 64% implying that this amino acid is not essential for activity (Lahti et al., 1991). Also in contrast to chemical modification studies, mutagenesis experiments on E-PPase have demonstrated that both Glu 98 and Glu 101 located in the "acidic hexapeptide" are perhaps unimportant for enzymatic activity (Cooperman et al., 1992). The other 2 residues, Lys 29 and Arg 43 in T-PPase (Lys 56 and Arg 78 in Y-PPase), are in a position to bind substrate as observed in the present crystal structure. Even conservative mutations of these amino acids in E-PPase resulted in a dramatic loss of activity (Cooperman et al., 1992).

Other potentially important amino acids revealed by chemical modification of the enzyme have not been identified within the primary structure. These include histidine and tyrosine residues in E-PPase (Samejima et al., 1988) and B-PPase (Shiroya & Samejima, 1985), tryptophan in P-PPase (Kaneko et al., 1991) and E-PPase (Kaneko et al., 1993), serine (Avaeva et al., 1970), methionine (Yano et al., 1973), tryptophan (Negi et al., 1972), and histidine (Nazarova et al., 1972; Cooperman & Chiu, 1973b) in Y-PPase. Our data support these findings with respect to tyrosines that form the bottom of the active center. No evidence for involvement of histidine, serine, tryptophan, or methionine in substrate binding could be provided on the basis of the T-PPase crystal structure and sequence alignment with other PPases.

Kinetic studies on Y-PPase (Welsh et al., 1983) and E-PPase (Baykov et al., 1990) provided evidence for a common catalytic mechanism of these enzymes. The model of PP_i hydrolysis by PPase proposed by Cooperman et al. (1992) assumes general base activation of the attacking nucleophilic water and activation of the leaving phosphoryl group through metal-ion complexation and general acid catalysis. This scheme is consistent with the location of amino acid residues and solvent molecules in the active center of T-PPase. Arg 43 would evidently play a central role in anchoring the leaving P_i. The orientation of its guanidinium group is maintained by hydrogen bonds to Asp 42 and Glu 143. Comparison of amino acid sequences suggests that these interactions are conserved in all PPases. Tyr 139, which forms a hydrogen bond to the anion in the present structure, can serve as a proton donor for this P_i. It is difficult to be certain about a general base catalyst because there are several carboxylic groups surrounding the putative PP_i binding site. From geometrical considerations, this role can be taken by Glu 31 or Asp 70. Both residues are important for activity as shown by site-specific mutagenesis studies of E-PPase (Cooperman et al., 1992). The variant E31D retains only 6% of activity of the wild-type enzyme. No activity was detected for the D70E variant. A more definitive model of PPase catalysis must await further X-ray studies of enzyme complexes with substrates and substrate analogs.

Structural role of conserved amino acids

Amino acid sequences have been determined for soluble PPases from *Saccharomyces cerevisiae* (cytoplasmic, Kolakowski et al., 1988; mitochondrial, Lundin et al., 1991), *Schizosaccharomyces pombe* (Kawasaki et al., 1990), *Kluyveromyces lactis* (Stark & Milner, 1989), bovine retina (Yang & Wensel, 1992), *Arabidopsis thaliana* (Kieber & Signer, 1991), *E. coli* (Lahti et al., 1988), *Thermoplasma acidophilum* (Richter & Schäfer, 1992), thermophilic bacterium PS-3 (Ichiba et al., 1990), *Bacillus stearothermophilus* and *T. thermophilus* (Ishii K, Shibuya K, Kaji H, Satoh T, Teplyakov A, Obmolova G, Kuranova I, Samejima T, manuscript in prep.). Their alignment clearly shows 2 distinct groups with much higher similarity inside the groups than between them. One group includes eukaryotic enzymes (first 5 listed above) that share 70–85% sequence identity. Prokaryotic enzymes and PPase from *A. thaliana* constitute another group, which is characterized by a lower degree of similarity (41–48%). Sequence similarity between members of the different groups does not exceed 27%.

All 10 sequences were aligned on the basis of the 3-dimensional superposition of T-PPase and Y-PPase. Figure 2 shows the sequences of T-PPase, Y-PPase (cytoplasmic), and E-PPase as representatives of the 2 groups of PPases. This alignment differs in some minor details from that of Lahti et al. (1990a) who compared Y-PPase and E-PPase. The differences mainly relate to secondary-structure elements present in only one of the proteins (e.g., α-helix 174–177 and 3_{10}-helix 204–207 in Y-PPase). The alignment of all active-site residues remains the same.

Twenty-two amino acid residues are strictly conserved in all PPases. Beside the 16 active-site residues, there are only 6 other amino acids that have been conserved during evolution and that therefore might be of structural importance for the enzyme. These include 3 glycines (56, 82, and 91 in T-PPase numbering), which support the β-barrel formation: Gly 56 and Gly 91 facilitate bending of β-strands 4 and 6; Gly 82 releases tension in the short loop connecting strands 5 and 6. Because this loop forms the β-turn of type II with Gly 82 in the $(i+2)$ position, it is likely that this secondary-structure element is conserved in the PPase family. All 3 glycines adopt a conformation that would be unfavorable for non-glycine residues (Fig. 9). Conservative Thr 61 is also related to the β-barrel structure (Fig. 1). Its methyl group contributes to the hydrophobic interior of the barrel, whereas its hydroxyl group bridges β-strands 4 and 5 through hydrogen bonds to the main-chain atoms. This should help to fix the ends of the loop, which donates 3 aspartyl residues (65, 67, and 70) to the active center. Conserved Pro 68 might be important for maintaining the rigidity of the loop. Phe 136 is a part of the aromatic cluster at the bottom of the active center.

Oligomeric structure

Typically for prokaryotic PPases, T-PPase forms hexamers under physiological conditions (Kuranova et al., 1987). In the crystal, the hexameric molecule of the enzyme occupies a unique position at the intersection of the 3-fold and 2-fold axes, so that the molecular symmetry (32) coincides with the crystallographic

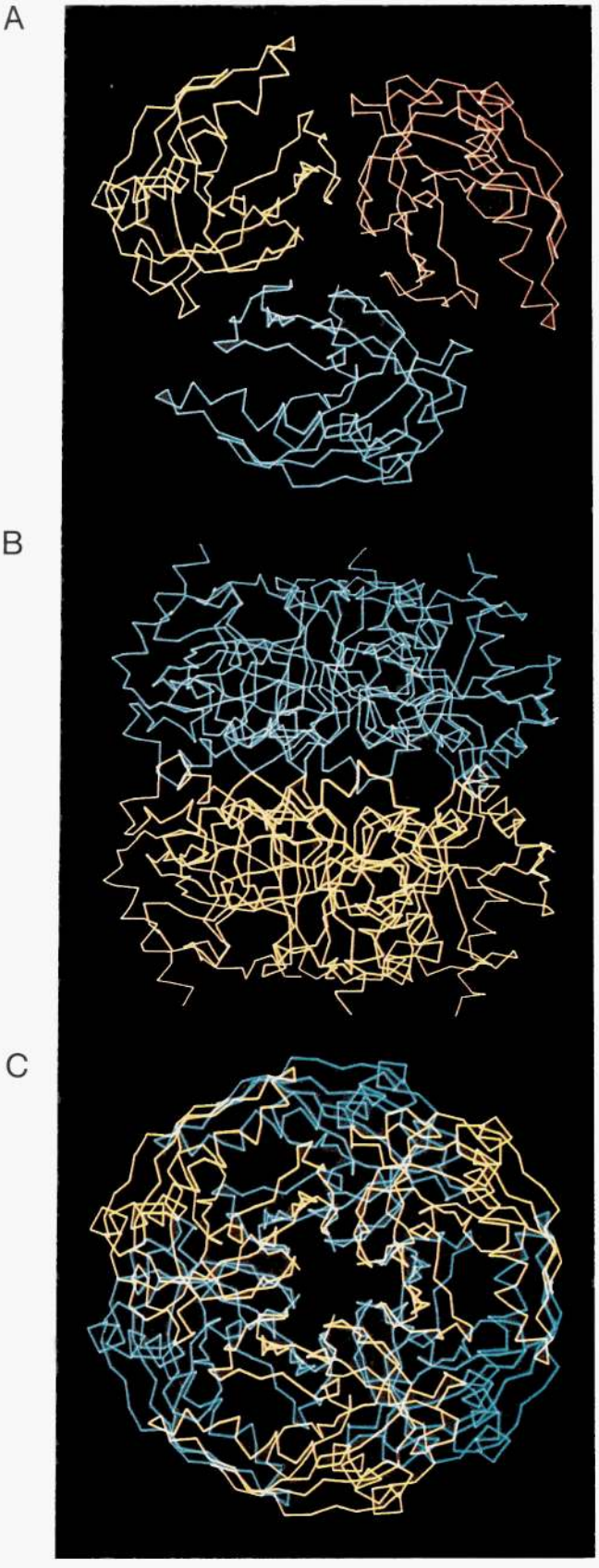

Fig. 7. Oligomeric structure of T-PPase. C_α-backbones are shown for (**A**) the trimer along the 3-fold axis and (**B**, **C**) the hexamer across and along the 3-fold axis, respectively.

symmetry. The hexamer is composed of 2 trimers and can be approximated by a cylinder with a diameter of 62 Å and height of 60 Å (Fig. 7). The upper trimer is rotated by 30° with respect to the lower one. This indicates the closest packing of the subunits composing the T-PPase hexamer. Electron microscopic studies of negatively stained preparations of E-PPase (Wong et al., 1970) revealed 2 forms of aggregates. Spherical particles 65 Å in diameter that dominated at pH 7 correspond to the compact hexameric structure found in T-PPase crystals. The other form observed at lower pH was a toroidal structure of 130–140 Å in diameter.

Interactions between subunits in the trimer are very tight. A parallel β-bridge between strand 6 of the β-barrel of one subunit and the β-hairpin of the other links together these 2 substructures to make a continuous 8-stranded β-sheet. In addition, there are 4 more hydrogen bonds at each intersubunit contact (Table 2). Together with extensive hydrophobic interactions, which include leucines 6, 36, 41, 79, 80, valines 44, 83, 85, 109, Pro 81, and tyrosines 30 and 77, these contacts provide the stability of the trimer. As shown for hexameric E-PPase, B-PPase, and P-PPase, the enzyme dissociates into active trimers and then to monomers rather than to dimers (Borschik et al., 1985; Ichiba et al., 1990).

The trimer–trimer interface is formed mainly by the symmetry-related α-helices A. The contacts between them are provided by side chains located on 1 side of the helix: Gln 130, His 134, Thr 138, and Leu 142 (Fig. 8). With the exception of Leu 142, these residues are not strictly conserved in hexameric PPases. This fact reflects the nonspecific character of the interaction, which is similar to a leucine zipper. Substitution of residues corresponding to His 134 and Thr 138 by site-directed mutagenesis was shown to influence the stability of E-PPase (Cooperman et al., 1992). This is not surprising because these 2 residues occupy the central position in the intertrimer "zipper" and form a hydrogen bond (Table 2).

Although nearly all PPases are oligomeric proteins, only the yeast enzyme has been shown to be allosteric (Cooperman & Chui, 1973a, 1973b). This does not imply, however, that allosteric regulation is uncommon for PPases because most kinetic studies have been carried at high concentration of Mg^{2+} acti-

Table 2. *Intersubunit hydrogen bonds*

H bonds	Distance (Å)
Intratrimer	
ND2 Asn 28···O Pro 78	3.18
O Ile 39···N Val 84	2.95
NZ Lys 40···OE1 Glu 86	3.32
N Leu 41···O Val 84	2.83
N Val 44···O Glu 111	3.23
O Leu 45···NH1 Arg 114	2.86
O Leu 45···NH2 Arg 114	2.93
O Gly 47···NH2 Arg 114	3.17
Intertrimer	
OE1 Gln 130···NZ Lys 145	2.99
NE2 Gln 130···OE1 Gln 113	3.32
OE2 Glu 131···NH2 Arg 114	2.81
NE2 His 134···O Thr 138	3.19

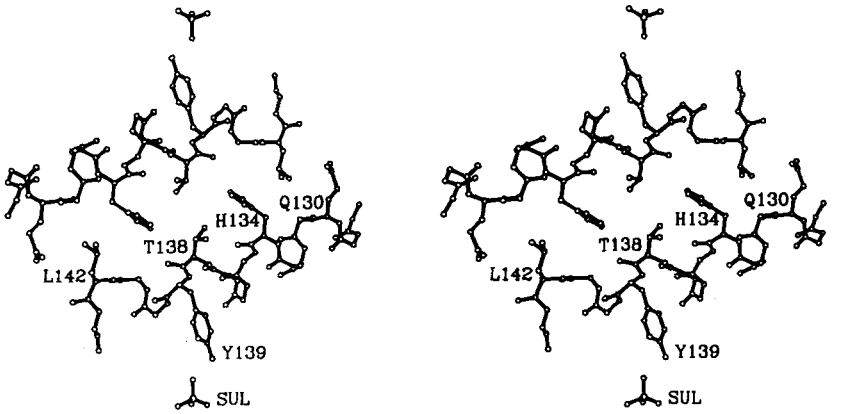

Fig. 8. Interaction between the active centers related by a 2-fold axis. Residue numbers are given for 1 subunit.

vator when even "allosteric PPases" would behave according to Michaelis–Menten kinetics (Lahti, 1983). Although all 6 active sites in the T-PPase hexamer are completely open and located at a large distance from each other (about 30 Å as measured between symmetry-related sulfate ions), one cannot rule out the possibility of allosteric behavior of the enzyme because there might be an interaction between active centers of the subunits related by a 2-fold axis. The signal-transfer mechanism would include helices A forming a trimer–trimer interface and Tyr 139 located at the C-terminus of this helix and involved in substrate binding (Fig. 8). Due to the rigid character of an α-helix, even slight changes in the orientation of Tyr 139 could cause shifts of helix A. From this point of view, one can explain the observed decrease of activity in H136Q (by 30%) and H140Q (by 75%) variants of E-PPase (Cooperman et al., 1992). These residues are part of the intersubunit "zipper" and their replacement might influence the position of helix A and subsequently of essential Tyr 139. Further studies are required to establish the allosterism of hexameric PPases.

Materials and methods

T-PPase was isolated from *T. thermophilus* HB8 and purified as described (Obmolova et al., 1993). Crystals suitable for X-ray analysis have been obtained by vapor diffusion from 15 mg/mL protein solution in 20 mM Tris-HCl buffer, pH 7.5, containing 47% ammonium sulfate, 3% 2-methyl-2,4-pentanediol, and 2 mM $MgSO_4$ (Obmolova et al., 1993). They belong to the rhombohedral space group R32 with $a = 110.3$, $c = 82.0$ Å, and contain one 20-kDa subunit in the asymmetric part of the unit cell. X-ray diffraction data to 2 Å resolution (11,673 unique reflections) were collected using a Syntex $P2_1$ diffractometer with a copper sealed tube. The data are 90% complete.

The structure of T-PPase was solved by molecular replacement using the unrefined atomic model of Y-PPase determined at 3.0 Å resolution (Terzyan et al., 1984; Protein Data Bank entry 1PYP). The model was modified according to the amino acid sequence alignment of Y-PPase and E-PPase (Lahti et al., 1990a); the primary structure of T-PPase (Ishii et al., manuscript in prep.) became available later at the stage of crystallographic refinement of the model. With respect to both T-PPase and E-PPase, the sequence of Y-PPase contains 82 extra residues at the N- and C-termini, and 28 extra residues in 7 insertions, all of which occur in loop regions (Fig. 2). Several probe models differing in the number of residues were tried until a solution was obtained for a model containing only the β-structural part of the Y-PPase molecule. Side chains on the surface of the molecule were truncated to C_β atoms. This model contained 706 atoms or 52% of the expected number of atoms in T-PPase. The structure was solved with the program package AMORE (Navaza, 1992). Several highest peaks on the rotation function were selected for the subsequent translation search. The top solution characterized by a correlation coefficient of 24% and an R-factor of 51% (10–3 Å, after rigid-body refinement) was correct. However, virtually the same values were obtained for a number of incorrect solutions. The correctness of the solution was justified by reasonable crystal packing and verified during refinement of the structure.

The initial electron density map was hardly interpretable. It improved gradually during molecular dynamics and conventional refinement using the programs XPLOR (Brünger et al., 1987) and PROLSQ (Hendrickson & Konnert, 1981). Manual correction of the model was performed using FRODO (Jones, 1985). The mean difference between initial phases and those cal-

Table 3. *Refinement statistics*

Parameter	RMSD (target σ)[a]
Bond distances (Å)	
1–2 Neighbors	0.015 (0.020)
1–3 Neighbors	0.036 (0.030)
1–4 Neighbors	0.046 (0.040)
Planar groups (Å)	0.013 (0.020)
Chiral volumes (Å^3)	0.162 (0.150)
Single torsion contacts (Å)	0.131 (0.300)
Multiple torsion contacts (Å)	0.189 (0.300)
Torsion angles (degrees)	
Planar	2.3 (3.0)
Staggered	18.1 (15.0)
Orthonormal	21.5 (20.0)
Temperature factors (Å^2)	
Main chain	4.0 (4.0)
Side chain	6.3 (6.0)

[a] RMS deviations from standard values are given. Values in parentheses are the inverse square root of the least-squares weights used for refinement.

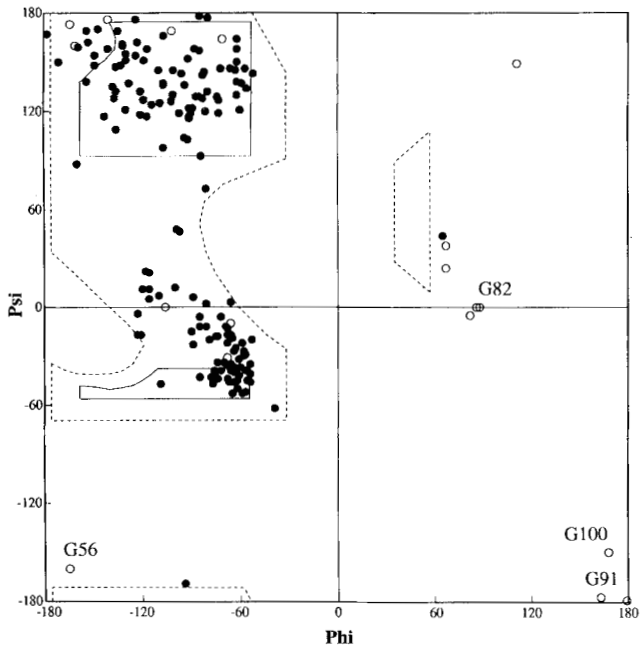

Fig. 9. (ϕ/ψ) plot of the atomic model of T-PPase. Glycine residues are shown as open circles. Conservative glycines are labeled.

culated from the final model was 72° in the resolution range 10–3 Å (80° in the range 10–2 Å). At the end of refinement, water molecules were added on the basis of ($F_o - F_c$) electron density maps. Each water molecule was required to lie within 3.5 Å from a potential hydrogen bond donor/acceptor. Their occupancies were set to unity and were not refined. Water molecules with B-factors greater than 50 Å^2 were excluded from the model.

The final electron density allowed modeling of all 174 amino acid residues in agreement with the primary structure of T-PPase. The model has been refined to an R-factor of 15.3% calculated for all measured reflections in the resolution range

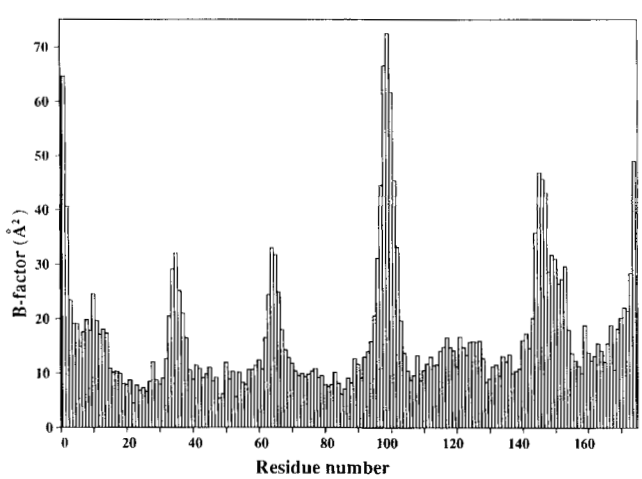

Fig. 10. B-factors averaged over the main-chain atoms as a function of residue number.

10.0–2.0 Å. The model of 1 subunit consists of 1,347 protein atoms, 1 sulfate ion, and 90 water molecules. The stereochemical parameters of the model are given in Table 3. The overall coordinate error in atomic positions derived from the σ_A plot (Read, 1986) is 0.19 Å. The ϕ/ψ plot (Fig. 9) shows no residues with forbidden combinations of main-chain torsion angles. One residue in T-PPase, Pro 13, is in the *cis*-conformation. It is located in a reverse turn of the polypeptide chain.

The mean B-factor calculated for all protein atoms is 19.2 Å^2. B-factors averaged over the main-chain atoms are represented in Figure 10. Only the N- and C-terminal residues and a couple of loops are slightly disordered: their atomic B-factors go up to 40–60 Å^2. For the rest of the structure, the electron density is well defined, reflecting the overall rigidity of the T-PPase subunit.

Atomic coordinates and structure factors have been deposited with the Brookhaven Protein Data Bank (Bernstein et al., 1977) under entry names 2PRD and R2PRDSF.

Acknowledgments

We thank Dr. Yu. Nekrasov for collecting X-ray data on a Syntex diffractometer and Drs. Z. Dauter and A. Murzin for helpful discussions.

References

Acharya KR, Passalacqua EF, Jones EY, Harlos K, Stuart DI, Brehm RD, Tranter HS. 1994. Structural basis of superantigen action inferred from crystal structure of toxic-shock syndrome toxin-1. *Nature 367*:94–97.

Avaeva SM, Nazarova TI, Vorobyeva NN. 1970. Interaction of inorganic pyrophosphatase with diisopropylfluorophosphate. *Biokhimiya 35*: 1113–1117.

Baykov AA, Shestakov AS, Kasho VN, Vener AV, Ivanov AH. 1990. Kinetics and thermodynamics of catalysis by the inorganic pyrophosphatase of *Escherichia coli* in both directions. *Eur J Biochem 194*:879–887.

Baykov AA, Shestakov AS, Pavlov AR, Smirnova IN, Larionov VN, Avaeva SM. 1989. The interaction of phosphate and manganese ions with baker's yeast inorganic pyrophosphatase. *Biokhimiya 54*:796–803.

Bernstein FC, Koetzle TF, Williams GJB, Meyer EF Jr, Brice MD, Rogers JR, Kennard O, Shimanouchi T, Tasumi M. 1977. The Protein Data Bank: A computer-based archival file for macromolecular structures. *J Mol Biol 122*:535–542.

Bond MW, Chiu NY, Cooperman BS. 1980. Identification of an arginine important for enzymatic activity within the covalent structure of yeast inorganic pyrophosphatase. *Biochemistry 19*:94–102.

Borschik IB, Pestova TV, Sklyankina VA, Avaeva SM. 1985. The quaternary structure of *E. coli* inorganic pyrophosphatase is not required for catalytic activity. *FEBS Lett 184*:65–67.

Brayer GD, McPherson A. 1983. Refined structure of the gene 5 DNA binding protein from bacteriophage fd. *J Mol Biol 169*:565–596.

Brünger AT, Kuriyan J, Karplus M. 1987. Crystallographic R factor refinement by molecular dynamics. *Science 235*:458–460.

Burton PM, Hall DC, Josse J. 1970. Constitutive inorganic pyrophosphatase of *Escherichia coli*. IV. Chemical studies of protein structure. *J Biol Chem 245*:4346–4352.

Butler LG. 1971. Yeast and other inorganic pyrophosphatases. In: Boyer PD, ed. *The enzymes, 3rd ed, vol 4*. New York: Academic Press. pp 529–541.

Chirgadze NY, Kuranova IP, Nevskaya NA, Teplyakov AV, Wilson KS, Strokopytov BV, Harutyunyan EH, Höhne WE. 1991. Crystal structure of MnP_i complex of yeast inorganic pyrophosphatase at 2.35 Å resolution. *Kristallografiya 36*:128–132.

Cooperman BS. 1982. The mechanism of action of yeast inorganic pyrophosphatase. *Methods Enzymol 87*:526–548.

Cooperman BS, Baykov AA, Lahti R. 1992. Evolutionary conservation of the active site of soluble inorganic pyrophosphatase. *Trends Biochem Sci 17*:262–266.

Cooperman BS, Chiu NY. 1973a. Yeast inorganic pyrophosphatase. II. Magnetic resonance and steady-state kinetic studies of metal ion and pyrophosphate analog binding. *Biochemistry 12*:1670–1676.

Cooperman BS, Chiu NY. 1973b. Yeast inorganic pyrophosphatase. III. Ac-

tive site mapping by electrophilic reagents and binding measurements. *Biochemistry 12*:1676–1682.

Cooperman BS, Panackal A, Springs B, Hamm DJ. 1981. Divalent metal ion, inorganic phosphate, and inorganic phosphate analogue binding to yeast inorganic pyrophosphatase. *Biochemistry 20*:6051–6060.

Gonzalez MA, Cooperman BS. 1986. Glutamic acid-149 is important for enzymatic activity of yeast inorganic pyrophosphatase. *Biochemistry 25*:7179–7185.

Hendrickson WA, Konnert JH. 1981. Stereochemically restrained crystallographic least-squares refinement of macromolecular structures. In: Srinivasan R, ed. *Biomolecular structure, conformation, function and evolution, vol 1*. Oxford, UK: Pergamon Press. pp 43–57.

Herbomel P, Ninio J. 1980. Fidelity of a polymerization reaction in relation to proximity to equilibrium. *C R Acad Sci D 291*:881–884.

Höhne WE, Wessner H, Kuranova IP, Obmolova GV. 1988. Kinetic characterization of a thermostable inorganic pyrophosphatase from *Thermus thermophilus*. *Biomed Biochim Acta 47*:941–947.

Ichiba T, Takenaka O, Samejima T, Hachimori A. 1990. Primary structure of the inorganic pyrophosphatase from thermophilic bacterium PS-3. *J Biochem 108*:572–578.

Jones A. 1985. Interactive computer graphics: FRODO. *Methods Enzymol 115*:157–171.

Josse J, Wong SCK. 1971. Inorganic pyrophosphatase from *Escherichia coli*. In: Boyer PD, ed. *The enzymes, 3rd ed, vol 4*. New York: Academic Press. pp 499–527.

Kabsch W, Sander C. 1983. Dictionary of protein secondary structure: Pattern recognition of hydrogen bonded and geometrical features. *Biopolymers 22*:2577–2637.

Kaneko S, Ichiba T, Hirano N, Hachimori A. 1991. Modification of a single tryptophan of the inorganic pyrophosphatase from thermophilic bacterium PS-3: Possible involvement in its substrate binding. *Biochim Biophys Acta 1077*:281–284.

Kaneko S, Ichiba T, Hirano N, Hachimori A. 1993. Modification of tryptophan-149 of inorganic pyrophosphatase from *Escherichia coli*. *Int J Biochem 25*:233–238.

Kawasaki I, Adachi N, Ikeda H. 1990. Nucleotide sequence of *S. pombe* inorganic pyrophosphatase. *Nucleic Acids Res 18*:5888.

Kieber JJ, Signer ER. 1991. Cloning and characterization of an inorganic pyrophosphatase gene from *Arabidopsis thaliana*. *Plant Mol Biol 16*:345–348.

Knight WB, Dunaway-Mariano D, Ransom SC, Villafranca JJ. 1984. Investigations of the metal ion-binding sites of yeast inorganic pyrophosphatase. *J Biol Chem 259*:2886–2895.

Kolakowski LF, Schlösser M, Cooperman BS. 1988. Cloning, molecular characterization and chromosome localization of the inorganic pyrophosphatase (PPA) gene from *S. cerevisiae*. *Nucleic Acids Res 22*:10441–10452.

Komissarov AA, Makarova IA, Sklyankina VA, Avaeva SM. 1985. The functionally important lysine residue in inorganic pyrophosphatase from yeast. *Bioorg Khimiya 11*:1504–1509.

Komissarov AA, Spanchenko OV, Sklyankina VA, Avaeva SM. 1987. The functionally significant residue of lysine in inorganic pyrophosphatase from *E. coli*. I. Interaction of inorganic pyrophosphatase with pyridoxal-5′-phosphate. *Bioorg Khimiya 13*:592–598.

Kraulis P. 1991. MOLSCRIPT: A program to produce both detailed and schematic plots of protein structures. *J Appl Crystallogr 24*:946–950.

Kuranova IP, Obmolova GV, Konareva NV. 1987. Inorganic pyrophosphatase from the extremely thermophilic bacterium *Thermus thermophilus* HB8. *Dokl Akad Nauk SSSR 295*:1013–1016.

Kuranova IP, Terzyan SS, Voronova AA, Smirnova EA, Vainshtein BK, Höhne WE, Hansen G. 1983. Active site structure of the inorganic pyrophosphatase from baker's yeast based on the X-ray investigation. *Bioorg Khim 9*:1611–1619.

Lahti R. 1983. Microbial inorganic pyrophosphatases. *Microbiol Rev 47*:169–179.

Lahti R, Kolakowski LF Jr, Heinonen J, Vihinen M, Pohjanoksa K, Cooperman BS. 1990a. Conservation of functional residues between yeast and *E. coli* inorganic pyrophosphatases. *Biochim Biophys Acta 1038*:338–345.

Lahti R, Pitkäranta T, Valve E, Ilta I, Kukko-Kalske E, Heinonen J. 1988. Cloning and characterization of the gene encoding inorganic pyrophosphatase of *Escherichia coli* K-12. *J Bacteriol 170*:5901–5907.

Lahti R, Pohjanoksa K, Pitkäranta T, Heikinheimo P, Salminen T, Meyer P, Heinonen J. 1990b. A site-directed mutagenesis study on *Escherichia coli* inorganic pyrophosphatase. Glutamic acid-98 and lysine-104 are important for structural integrity, whereas aspartic acids-97 and -102 are essential for catalytic activity. *Biochemistry 29*:5761–5766.

Lahti R, Salminen T, Latonen S, Heikinheimo P, Pohjanoksa K, Heinonen J. 1991. Genetic engineering of *Escherichia coli* inorganic pyrophosphatase. Tyr 55 and Tyr 141 are important for the structural integrity. *Eur J Biochem 198*:293–297.

Lundin M, Baltscheffsky H, Ronne H. 1991. Yeast *PPA2* gene encodes a mitochondrial inorganic pyrophosphatase that is essential for mitochondrial function. *J Biol Chem 266*:12168–12172.

McLachlan AD. 1979. Gene duplications in the structural evolution of chymotrypsin. *J Mol Biol 128*:49–79.

Moroz OV, Strokopytov BV, Oganesyan VY, Airumyan LG, Nekrasov YV, Nazarova TI, Kurilova SA, Vorobyeva NN, Terzyan SS, Avaeva SM, Arutyunyan EG. 1991. Investigation of inorganic pyrophosphatase from *E. coli* at a resolution of 5 Å. *Kristallografiya 36*:454–458.

Murzin AG. 1993. OB (oligonucleotide/oligosaccharide binding)-fold: Common structural and functional solution for non-homologous sequences. *EMBO J 12*:861–867.

Navaza J. 1992. AMORE: A new package for molecular replacement. In: Dodson EJ, Gover S, Wolf W, eds. *Molecular replacement. Proceedings of the CCP4 study weekend*. Daresbury, UK: SERC Daresbury Laboratory. pp 87–90.

Nazarova TI, Fink NY, Avaeva SM. 1972. Phosphohistidine as the result of phosphate migration in phosphorylated inorganic pyrophosphatase from yeast. *FEBS Lett 20*:167–168.

Negi T, Samejima T, Irie M. 1972. Studies on the tryptophan residues of yeast inorganic pyrophosphatase in relation to the enzymatic activity. *J Biochem 71*:29–37.

Obmolova G, Kuranova I, Teplyakov A. 1993. Purification and preliminary X-ray analysis of inorganic pyrophosphatase from *Thermus thermophilus*. *J Mol Biol 232*:312–313.

Orengo CA, Thornton JM. 1993. Alpha plus beta folds revisited: Some favoured motifs. *Structure 1*:105–120.

Prasad GS, Earhart CA, Murray DL, Novick RP, Schlievert PM, Ohlendorf D. 1993. Structure of toxic shock syndrome toxin 1. *Biochemistry 32*:13761–13766.

Raznikov AV, Egorov TA, Mirgorodskaya OA, Sklyankina VA, Avaeva SM. 1992a. Essential glutamic acid residue in *E. coli* pyrophosphatase. 1. Chemical modification and localization within the primary structure. *Biokhimiya 57*:1324–1332.

Raznikov AV, Sklyankina VA, Avaeva SM. 1992b. Tyrosine-89 is important for enzymatic activity of *S. cerevisiae* inorganic pyrophosphatase. *FEBS Lett 308*:62–64.

Read RJ. 1986. Improved Fourier coefficients for maps using phases from partial structures with errors. *Acta Crystallogr A 42*:140–149.

Richardson JS. 1981. The anatomy and taxonomy of protein structure. *Adv Protein Chem 34*:167–339.

Richter OM, Schäfer G. 1992. Cloning and sequencing of the gene for the cytoplasmic inorganic pyrophosphatase from the thermoacidophilic archaebacterium *Thermoplasma acidophilum*. *Eur J Biochem 209*:351–355.

Samejima T, Tamagawa Y, Kondo Y, Hachimori A, Kaji H, Takeda A, Shiroya Y. 1988. Chemical modifications of histidyl and tyrosyl residues of inorganic pyrophosphatase from *Escherichia coli*. *J Biochem 103*:766–772.

Schindelin H, Marahiel MA, Heinemann U. 1993. Universal nucleic acid-binding domain revealed by crystal structure of the *B. subtilis* major cold-shock protein. *Nature 364*:164–168.

Schnuchel A, Wiltschek R, Czisch M, Herrier M, Willimsky G, Graumann P, Marahiel MA, Holak TA. 1993. Structure in solution of the major cold-shock protein from *Bacillus subtilis*. *Nature 364*:169–171.

Shestakov AA, Baykov AA, Avaeva SM. 1990. Tightly bound pyrophosphate in *Escherichia coli* inorganic pyrophosphatase. *FEBS Lett 262*:194–196.

Shiroya Y, Samejima T. 1985. The specific modification of histidyl residues of inorganic pyrophosphatase from *Bacillus stearothermophilus* by photooxidation. *J Biochem 98*:333–339.

Stark MJR, Milner JS. 1989. Cloning and analysis of the *Kluyveromyces lactis TRP1* gene: A chromosomal locus flanked by genes encoding inorganic pyrophosphatase and histone H3. *Yeast 5*:35–50.

Terzyan SS, Voronova AA, Smirnova EA, Kuranova IP, Nekrasov YV, Arutyunyan EG, Vainshtein BK, Höhne WE, Hansen G. 1984. Structure of yeast inorganic pyrophosphatase at 3.0 Å resolution. *Bioorg Khim 10*:1469–1482.

Welsh KM, Jakobyansky A, Springs B, Cooperman BS. 1983. Catalytic specificity of yeast inorganic pyrophosphatase for magnesium ion as a cofactor. An analysis of divalent metal ion and solvent isotope effects on enzyme function. *Biochemistry 22*:2243–2248.

Wong SCK, Hall DC, Josse J. 1970. Constitutive inorganic pyrophosphatase of *Escherichia coli*. III. Molecular weight and physical properties of the enzyme and its subunits. *J Biol Chem 245*:4335–4345.

Yang ZH, Wensel TG. 1992. Molecular cloning and functional expression of cDNA encoding a mammalian inorganic pyrophosphatase. *J Biol Chem 267*:24641–24647.

Yano Y, Negi T, Ire M. 1973. Carboxamidomethylation of yeast inorganic pyrophosphatase. *J Biochem 74*:67–76.